Title

Pressure-activated microsyringe (PAM) fabrication of bioactive glass/poly(lactic-co-glycolic acid) composite scaffolds for bone tissue regeneration

Short Title

PAM fabrication of bioactive glass/PLGA composite scaffolds

M. Mattioli-Belmonte[1*], C. De Maria[2*], C. Vitale-Brovarone[3], F. Baino[3], M. Dicarlo[1], G. Vozzi[2,4]

* Both Authors equally contributed to the research.

[1]Department of Clinical and Molecular Sciences, Università Politecnica delle Marche, Ancona, Italy.

[2]Research Centre "E. Piaggio" - University of Pisa, Pisa, Italy

[3]Institute of Materials Physics and Engineering, Politecnico di Torino, Turin, Italy

[4]Dipartimento di Ingegneria dell'Informazione, University of Pisa, Pisa, Italy

Correspondence to:

Prof. Giovanni Vozzi

Research Centre "E. Piaggio"

University of Pisa

Largo Lucio Lazzarino, 2

56126 Pisa, Italy

Abstract

The aim of this work was the fabrication and characterization of bioactive glass/poly(lactic-*co*-glycolic acid) (PLGA) composite scaffolds mimicking the topological features of cancellous bone. Porous multilayer PLGA/CEL2 composite scaffolds were innovatively produced by pressure activated microsyringe (PAM) method, a CAD/CAM processing technique originally developed at the University of Pisa. In order to select the optimal formulations to be extruded by PAM, CEL2/PLGA composite films (CEL2 is an experimental bioactive SiO_2-P_2O_5-CaO-MgO-Na_2O-K_2O glass developed at Politecnico di Torino) were produced and mechanically tested. The elastic modulus of the films increased from 30 to above 400 MPa increasing the CEL2 amount (10-50 wt.%) in the composite. The mixture containing 20 wt.% CEL2 was used to fabricate 2D and 3D bone-like scaffolds composed by layers with different topologies (square, hexagonal and octagonal pores). It was observed that the increase of complexity of 2D topological structures led to an increment of the elastic modulus from 3 to 9 MPa in the composite porous monolayer. The elastic modulus of 3D multilayer scaffolds was intermediate (about 6.5 MPa) between the values of the monolayers with square and octagonal pores (corresponding to the lowest and highest complexity, respectively). MG63 osteoblast-like cells and periosteal derived precursor cells (PDPCs) were used to assess the 3D bone-like scaffolds biocompatibility. A significant increase in cell proliferation from 48 h to 7 days of culture was observed for both cell phenotypes. Moreover qRT-PCR analysis evidenced an induction of early genes of osteogenesis in PDPCs.

Keywords: CEL2 bioactive glass, PAM system, cancellous bone structures, mechanical and topological characterisation, MG63 osteoblast-like cells and periosteal derived precursor cells, qRT-PCR analysis

1. Introduction

In the field of orthopaedics, which counts approximately 10 million surgeries related to bone fixation or articular cartilage injuries worldwide per year (WHO Technical Report Series, 2003), regenerative medicine offers significant therapeutic advantages and may even lead to active and sustained repair (Williams, 2006), and a first generation of orthopaedic products has been delivered to the clinics: these products are based on mature cells in suspension, encapsulated in hydrogels, or seeded into three-dimensional (3D) porous matrices (scaffolds) (Behrens et al, 2006; Sharma et al, 2007; Pavesio et al, 2003; Brittberg et al, 2003). Scaffolds are needed to lodge cells and provide a temporary template for tissue formation, development and maturation. To date, a number of 3D scaffolds with random architectural and structural properties have been brought to the market. These implants restore tissue functionality while reducing pain (Pavesio et al, 2003; Brittberg et al, 2003; Pietrzak et al, 2005). Although first clinical trials revealed promising initial responses after implantation, long-term follow-up studies showed the occurrence of degeneration and lack of integration with the surrounding tissues, thus leading to the need of another implant (Pavesio et al, 2003; Pietrzak et al, 2005).

In order to develop a functional and bioactive scaffold able to promote, drive and control tissue renewal, it is important to take into account three key factors: 1) the use of a biomaterial with enhanced biocompatibility and bioactivity; 2) a material processing method able to mimic tissue topology; and 3) a scaffold topology able to simulate the mechanical features of native tissue in the early stage of development as demonstrated by Engler (Murphy et al, 2014).

In the last few decades, a number of resorbable synthetic and natural polymers have been investigated as biomaterials for bone tissue engineering and regenerative medicine applications: materials such as poly(lactic acid), polycaprolactone, poly(glycolic acid), polyurethanes or their combinations, have been widely utilised (Mattioli-Belmonte et al, 2008; Rossi et al, 2013). Indeed, they present limited (e.g. just adhesive groups) or no presence of bioactive moieties to

improve the biocompatibility and this fact greatly limits their regenerative capacity. This drawback can be principally overcome by either functionalizing the external surface of a scaffold or by simply mixing growth factors into the bulk material, thus making them available with the biomaterial degradation (Ciardelli et al, 2010). Biologically derived proteinaceous materials such as collagen, fibrin or glycosaminoglycans (e.g. hyaluronic acid) have also been used (Jelen et al, 2013; Ranjangam et al, 2013; Kruger et al, 2013; Vindigni et al, 2009).

A recent approach is to combine different materials to produce a composite structure. Composite scaffolds are expected to be physically and biologically better than single material based scaffolds, as the properties of a composite may be tuned mixing different materials in various ratios (Gloria et al, 2010). Both the composition and the relative ratio of constituent materials can affect bone formation. Hydroxyapatite (HA) has been used as a primary material combined with tricalcium phosphate (TCP), poly(lactic-*co*-glycolic acid) (PLGA), or chitin, to produce different composite scaffolds (Boccaccini et al, 2005). Scaffolds with different ratios of HA:TCP loaded with mesenchymal stem cells (MSCs) showed different extents of bone formation in vivo (Siggers et al, 2010); composites in which the HA:TCP ratio was designed to coordinate scaffold degradation with tissue deposition were able to promote ectopic bone formation (Yang et al, 2014). In recent years, bone scaffolds based on carbon nanotubes (CNTs) have also been proposed (Shi et al, 2007; Veetil et al, 2009; Coleman et al, 2004; Coleman et al, 2006; Liu et al, 2004; Mattioli-Belmonte et al, 2012; Whulanza et al, 2013).

The attention of researchers has also been attracted by the development of bioactive glass/polymer composites, as bioactive glasses can bond to host bone and stimulate new bone growth, making them ideal candidates for hard tissue engineering applications (Rezwan et al, 2006; Jones, 2009; Baino et al, 2011).

Once the most suitable biomaterial (in terms of control of cell functions) is selected, it is also important to be able to produce a 3D scaffold mimicking the bone tissue topology. The

fabrication of polymeric 3D structures with complex geometries is mostly based on Rapid Prototyping (RP), using computer aided design/computer aided manufacturing (CAD/CAM) systems. In general, the RP methods can be divided in two groups: (a) solid polymer and (b) liquid polymer microfabrication techniques (Vozzi et al, 2008). The first group (a) includes all the techniques where the polymeric grains are placed on the x-y plane of the system and the working head (laser, ink-jet head, etc.) builds up the microstructures (Thomson et al, 1996; Kawata et al, 2001). The second group (b) includes those techniques in which the polymer is dispensed through a tool-head mounted on an arm or on the z-axis of a computer-controlled 3D micropositioner. In this case, the attained resolution is generally a function of the viscosity of the polymeric system, the motor speed, the physical principle that allows polymer dispensing and the geometry of the nozzle (Tirella et al,2012; Vozzi et al, 2002;Vozzi et al, 2004; Mironov et al, 2003; Landers et al, 2002).

In this study, PLGA and a silicate bioactive glass have been used to fabricate 3D bone-like structures in order to analyse how the combination of a bioactive composite material and a well-defined topology similar to that of the natural tissue, is able to promote cell functions. To produce these microfabricated composite structures the bioactive inorganic phase was a silicate six-oxide glass (termed CEL2) belonging to the SiO_2-P_2O_5-CaO-MgO-Na_2O-K_2O system. In previous works, CEL2 was used mainly as a starting material for making sintered glass-ceramic 3D scaffolds with adequate mechanical properties for bone repair applications (Vitale-Brovarone et al, 2009) and excellent bioactive properties, even better than the ones of 45S5 Bioglass®, which is commonly considered as the "gold standard" (Baino et al, 2013; Renghini et al, 2013). CEL2 as such was also found to be bioactive *in vitro* (Miola et al, 2012) and, moreover, the coating of polyurethane porous matrices with CEL2 powder was considered suitable to stimulate HA formation after their contact with biological fluids (Baino et al, 2009).

The PLGA/CEL2 composite material was initially tested in terms of mechanical properties to evaluate how the variation of CEL2 concentration influences its elastic modulus. The composite with the optimal ratio of the two materials, selected on the basis of its mechanical and rheological properties, was then processed by a CAD/CAM system (pressure activated microsyringe, PAM). Using this system, 2D layers with different topologies and a 3D bone-like composite structure were produced and mechanically tested.

At last, human osteoblast-like cell line (MG63) and human periosteal derived precursor cells (PDPCs) were seeded on the 3D bone-like scaffolds in order to assess their adhesion, morphology and proliferation. PDPCs show a cell-surface marker profile similar to MSCs and are efficient cells for complex skeletal- tissue defect healing (Ferretti et al, 2014). To this aim, real time PCR and quantification of mRNA were performed to better understand how the scaffold influences these bone precursor cell activities.

Bioglass® is the most commonly used inorganic phase in the preparation of polymer/bioactive glass composites. More specifically, processing methods reported for producing PLGA/Bioglass® composite include thermally-induced phase separation, microsphere emulsification, solvent casting, infiltration/coating, and electrophoresis (Rezwan et al, 2006). Microfabrication of PLGA/CEL2 composite scaffolds by PAM is proposed in this work for the first time; furthermore, the strategy of producing these 3D composite scaffolds by combining 2D porous layers with different topological features is also novel.

2. Materials and methods

2.1 Synthesis of the glass powder

The selected glass CEL2 (molar percentage of the constituting oxides: 45% SiO_2, 3% P_2O_5, 26% CaO, 7% MgO, 15% Na_2O, 4% K_2O) was produced following a conventional melting-quenching process. Glass reagents (high-purity powders of SiO_2, $Ca_3(PO_4)_2$, $CaCO_3$, Na_2CO_3, $(MgCO_3)_4{\cdot}Mg(OH)_2{\cdot}5H_2O$ and K_2CO_3, purchased from Sigma-Aldrich) were molten in air at

1550 °C (heating rate set at 10 °C min^{-1}) in a platinum crucible, that was maintained at this temperature for 1 h to ensure homogeneity of the melt. The glass was then quenched in cold water to obtain a frit, that was subsequently ground by using a 6-ball zirconia milling jar and sieved (Giuliani stainless steel sieve) to obtain particles with size below 20 μm.

2.2 Production of Composite film

75/25 poly(D,L-lactic-*co*-glycolic acid) (PLGA, Lactel, Pelham AL USA, M_W = 18,000 Da) was dissolved in chloroform (Sigma Aldrich, Italy) with a concentration of 10 and 20 % (w/v). CEL2 particles were sonicated in chloroform for 2 minutes to obtain a homogenous dispersion for different concentration values. In particular, CEL2 disper-sions with concentrations of 1%, 2%, 3%, 4% and 5% w/vwere prepared to be mixed with the 10% w/v PLGA solu-tion, whereas CEL2 dispersions with concentrations of2%, 4%, 6%, 8% and 10% w/v were used to mix withthe 20% w/v PLGA solution. Various composite mixtures were obtained adding the CEL2 dispersion to the polymer solution in a volume ratio of 1:1 and further sonicating them for 2 minutes. The resulting CEL2:polymer weight ratios were of 10%, 20%, 30%, 40% and 50% (w/w). Composite films were obtained by casting the dispersion in glass petri dishes and then dried in a silica tank for seven days to allow the complete evaporation of solvents. The polymer film thickness was around 50 μm. The different compositions used to produce the films are summarized in Table 1. The preparation of the distinct composite films was necessary to evaluate which one of the different dispersions presented the mechanical properties more similar to those ones of native bone in the early stage of development (Murphy et al, 2014).

2.3 Mechanical testing of the films

The composite dried films were cut into rectangular-shaped samples of 20 mm x 10 mm. The mechanical properties of CEL2-containing materials were measured using Zwick/Roell testing device (Z005 series, Genova, Italy). In this test, each sample was pulled until 1% deformation was reached. The load was applied in the axial direction (in-plane) of the sample, while

stretching the specimen at a constant strain rate of 0.1 %/s. Load and elongation were recorded by a computer connected to the control unit of the tensile apparatus. The elastic modulus was estimated from the stress-strain graphs.

To analyse the viscoelastic behaviour, creep tests were performed using an isotonic transducer (7006 Ugo Basile, Italy) connected to an acquisition system (17400 Data Capsucle, Ugo Basile, Italy). On the basis of the obtained stress-strain graph, the load measured in correspondence of the 0.1% deformation was applied for 30 minutes and then removed for other 30 minutes in order to observe the deformation recovery of the structure. All data acquired in the mechanical tests were analysed with an *ad-hoc* program developed in Matlab® (The Mathworks Inc., MA, USA) environment.

2.4 Fabrication of Composite scaffold

Among the RP methods based on CAD/CAM systems, the PAM technique exploits the pressure-driven extrusion of a polymer solution through a capillary needle and allows the fabrication of two- and three-dimesional polymeric scaffolds with a very high resolution. This automated system was developed at the Research Center "E. Piaggio" of the University of Pisa in 2002 (Vozzi et al, 2002). The deposition unit consists of a stainless-steel syringe equipped with a 5–20 μm glass capillary needle through which a solution of the choosen polymer, in a volatile solvent, is extruded by the application of filtered compressed air. The polymer solution viscosity has to be in the range of 10-300 cP. An electronically controlled pressure valve is employed to apply a constant pressure, ranging between 10 and 300 mmHg, to the syringe. A 0.1 μm resolution three-axis micropositioner, designed and built in-house, allows the control of motors in terms of speed and position: the syringe is mounted on the z-axis of the motion system, whereas the x- and y-axis motors are used to move the supporting substrate, usually a glass plate, relative to the syringe position. The entire system – including valves, pressure regulators, sensors, and position controllers – is interfaced to, and controlled by, an IRIS card

(Eclipse, Pisa, Italy), which enables the control of motor speeds (i.e., up to 10 cm/s in both x and y directions) and position. The control software was written in the C language: its user-friendly graphic interface allows a variety of patterns with simple or complex geometries to be designed and deposited. The lateral dimensions of the deposited structures ranges from 5 to 600 μm, depending on the pressure applied to the syringe, the viscosity of the solution, the motor speed, and the internal diameter of the syringe tip. All these working parameters can be controlled through the user-interface. The system has been characterized and optimized, and a simple model simulating the fluid-dynamics of the deposition process has been developed (Vozzi et al, 2002; Mariani et al, 2006). More complex three-dimensional topologies can be produced by using a layer-by-layer deposition process and by moving the syringe up along the z-axis by an amount corresponding to the height of each layer. Different layers can be built with different polymers in several patterns, thus a wide range of 3D structures can be fabricated.

Using this system, 2D scaffolds with square, hexagonal and octagonal cell base units were fabricated. Then, a bone micro-CT was sliced and each slice was approximated to one of the three topologies described before; eventually, the final CAD design was uploaded in PAM system software and a 3D bone-like scaffold was built up. This structure, as described in (Mattioli-Belmonte et al, 2008), was composed of three layers, one having a hexagonal cell grid with cell sides of 500 μm, the second one having a square cell grid with cell sides of 500 μm and the third one was an octagonal/rhomboidal cell grid in which the octagonal cell had sides of 500 μm. A small rhomboid was required between the octagonal cells to ensure a tessellated structure. This combination of geometries was chosen because it is simple to fabricate and allows attaining a complex and well controlled, regular 3D architecture, similar to trabecular bone. The dimensions of the fabricated samples were 1 cm x 1 cm, with heights of a few tens of microns.

2.5 Mechanical testing of the scaffolds

The mechanical properties of the 2D and 3D composite PAM scaffolds were measured using Zwick/Roell testing device (Z005 series, Genova, Italy): the samples were pulled until rupture at a constant strain rate of 0.1 %/s with the load applied in the plane of the sample.

2.6 In vitro culture

MG-63 human osteoblast-like cells (ATCC, Rockville, MD) were grown in a controlled atmosphere (5% CO_2 at 37°C) in Dulbecco's Modified Eagle's Medium (DMEM, Sigma-Aldrich, Milan, Italy) supplemented with 10% foetal bovine serum (FBS), 1% non-essential aminoacids 2.0 mM L-glutamine and 1% penicillin-streptomycin (all from GIBCO, Life Technologies, Milan, Italy). After thawing, cells were routinely split 1:10 every 3-4 days and used between passages 3 and 4.

PDPCs were isolated from periosteal tissue of subjects undergoing surgery for orthopaedic trauma, after the obtainment of their informed consent, as previously described (Ferretti et al, 2012). Briefly, tissue was aseptically dissected, washed three times in PBS, cut into small pieces (2-3 mm x 2-3 mm) and placed into culture dish in Dulbecco's Modified Eagle Medium: Nutrient Mixture F-12 (DMEM/F12 Sigma-Aldrich), supplemented with 10% FBS and 1% penicillin-streptomycin (100 U/ml). The cells were then allowed to adhere in standard cell culture conditions in a controlled atmosphere (5% CO_2; 37°C). The medium was changed twice a week and cells at the 3rd passage of subculture were used. In order to assess PDPCs mesenchymal stem cells phenotype, cells were characterised by FACSCalibur flow cytometry system (Becton Dickinson, CA, USA), using antibodies against the following surface antigens: HLA-DR, CD34, CD105, CD14, CD19 and CD45 (Diaclone, Besancon, France); CD73 and CD90 (StemCell Technologies, Inc. Vancouver, BC, Canada) (Dominici et al, 2006).

2.7 Cell seeding

Before seeding, the 3D bone-like scaffolds were sterilized in 70% ethyl alcohol solution (ETOH; Sigma-Aldrich) for 2 h, washed two times in PBS (Gibco) for 30 min and placed under

UV 15 min for each side. In order to improve cell adhesion, scaffolds were then conditioned overnight in 10% serum added DMEM or DMEM/F12 at 5% CO_2, 37°C. The media were then discarded and scaffolds considered ready for seeding (Gentile et al, 2012). Cells were detached using 0.25% trypsin in 1 mM ethylene diamine tetra-acetic acid (EDTA, Sigma-Aldrich) and seeded at a density of $1x10^4$ cell/cm^3 by applying 50 µl of cell suspension on the samples placed in at 37°C for 30 min in a humidified chamber, in order to avoid the slip down of cells. Then 1.5 ml of the appropriate culture media was added to cover the samples placed in Corning® ultra-low attachment multiwell plates. Cells were cultured for 48 h and 7 days.

2.8 MTT (3-dimethylthiazol-2,5-diphenyltetrazolium bromide) colorimetric assay

After incubation (48 h and 7 days), the medium was removed; 200 µl of MTT solution (Sigma-Aldrich, 5 mg/ml in DMEM without phenol red) and 1.8 ml DMEM were added to the cell monolayer; the multi-well plates were incubated at 37°C for further 4 h. After discarding the supernatants, the dark blue Formosan crystals were dissolved by adding 2 ml of solvent (10% HCl 1 N in isopropanol, Sigma-Aldrich) and quantified spectrophotometrically (Secomam, Anthelie light, version 3.8, Contardi, Italy) at 570 nm and 690 nm. In the control cultures, the cells were placed directly into adherent polystyrene culture plates at the same culture density as placed onto the samples.

2.9 Scanning Electron Microscopy (SEM)

Samples from cell culture tests were fixed in 2% glutaraldehyde (Sigma-Aldrich) in 0.1 M cacodylate buffer, pH = 7.4 (Sigma-Aldrich), post-fixed in 1% osmium tetroxide (Sigma-Aldrich), dehydrated in increasing ethanol (Sigma-Aldrich) concentrations, CPD-dried, mounted on aluminium stubs, gold-sputtered by the Edwards Sputter Coater B150S equipment and observed with a Philips XL 20 SEM (FEI Italia SRL, Milan, Italy) microscope.

2.10 RNA extraction, quantitation and Reverse Transcription

Total RNA was isolated from PDPCs cultured onto the different scaffolds with TRIzol® Reagent [Life Technologies, Monza (MI), Italy], according to manufacturer's instructions.

Quantification and evaluation of RNA quality were performed by spectrophotometric analysis (bioPhotometer plus, Eppendorf GmbH, Germany); 1 µg total RNA was reverse transcribed in a 20 µl reaction volume, using The GoScript™ Reverse Transcription System (Promega, Italia). Neo-synthesized cDNA was stored at -20°C.

2.11 Real-Time PCR (RT-qPCR) Assay

Real-time assays were performed by Mastercycler realplex2 (Eppendorf GmbH, Germany) using SsoFast™ EvaGreen® Supermix 1X, in a final volume of 10 µl. All PCR reactions contained 1 µl of cDNA (corresponding to 50 ng total RNA template). Each PCR assay were performed in white plastic-ware and comprised 30 s at 95°C for enzyme activation, 40 cycles of denaturation at 95°C for 5 s, annealing and extension at 60°C for 20 s. Each primer was used at 200 nM final concentration. The primer sequences were designed by Primer 3 (v. 0.4.0) software and their specificity was tested by BLAST Assembled RefSeq Genomes in order to avoid any appreciable homology to pseudogenes or other unexpected targets. The oligonucleotide sequences for target genes are listed in Table 2.

In each assay, both reference genes and each gene of interest mRNA were measured simultaneously under identical conditions. The primers showed the same amplification efficiency. Specificity of the PCR reactions was furthermore confirmed by melt-curve analysis.

2.12 Quantification of mRNA Expression

Each assay was performed as triplicate and reference gene Cq values were used to normalize cellular mRNA data. In this instance normalization involved the ratio of mRNA concentrations of specific genes of interest (as mentioned above) to that of GAPDH Cq medium value. In order to analyse PDPCs gene expression onto scaffolds, the ΔΔCq method for the evaluation of Fold-Change was employed using periosteal cells cultured into tissue culture plates under osteogenic stimuli as control. The relative amount of each mRNA was calculated using the comparative threshold (Ct) method with $\Delta Ct = Ct(mRNA) - Ct(GAPDH)$ and relative quantification of

mRNA expression was calculated with the $2^{-\Delta\Delta Ct}$ method (Livak et al, 2001). The qPCR efficiency in all our experiments was > 90%. The difference between the actual and theoretical (100%) efficiencies would result in an underestimation of the mRNA concentration of all analysed samples.

Data in histograms are expressed as Fold-regulation that represents fold-change results in a biologically meaningful way. Fold-change values > 1 indicate an up-regulation, and the fold-regulation is equal to the fold-change. Fold-change values < 1 indicate a down-regulation, and the fold-regulation is the negative inverse of the fold-change.

2.13 Statistical analysis

Mean and standard deviation of three different experiments are reported. MTT and qRT-PCR data were analysed by one-way ANOVA, Student-Newman-Keuls and Student's T tests. Statistical significance was tested at $p<0.05$.

3. Results and discussion

3.1 Mechanical properties of composite films

As can be observed from mechanical testing of composite films produced with both 5 and 10% (w/v) concentration of PLGA in the final solution, their mechanical behaviour is approximately linear (Figure 1A and B), as indicated by the R^2 coefficient, whose minimum value is 0.97 in case of 5% w/v PLGA, 10% w/w CEL2:PLGA ratio and a maximum of 0.99 for 10% w/v PLGA, 50% w/w CEL2:PLGA ratio; furthermore, the elastic modulus increases with the CEL2:PLGA ratio (Figure 1C).

It can also be noted that the composite films produced with 5% w/v PLGA solution presented higher elastic moduli with respect to those realized with 10% (w/v) PLGA solution. This is probably due to the fact that by increasing the viscosity of PLGA solution, the CEL2 particles are not completely well dispersed in the mixture and create some clots that reduce the elastic modulus (Zhang du et al, 2009).

Starting from the analysis of the creep curve, we modelled the mechanical behaviour of the films with a solid linear standard model (Figure 2A, B), which predicts the deformation *ε(t)* in response to a constant load σ_0 as described by equation (1):

$$\varepsilon(t) = \frac{\sigma_0}{E_1}\left[1 + \frac{E_1}{E_2}\left(1 - e^{-\frac{t}{\tau}}\right)\right] \qquad \text{(eq. 1)}$$

where E_1 and E_2 are the spring's elastic constant, and τ is the characteristic time and is equal to:

$$\tau = \frac{\eta}{E_1 + E_2} \qquad \text{(eq. 2)}$$

with η that represents the viscosity parameter of the damper (Figure 2A).

This model fits with a very good approximation experimental data, as indicated by the coefficient R^2, which is always > 0.86. Comparing the data obtained by fitting the model with experimental data (Tables 3, 4) it is possible to note that the E_1 parameters can be related to the elastic modulus of polymer-based films that we evaluated from the stress-strain curve. A linear regression between the measured elastic modulus and E_1 gives a slope of 1.3 with an R^2 of 0.95 in case of 5% w/v PLGA and a slope of 0.995 with an R^2 of 0.99 in case of 10% w/v PLGA.

E_2 for 10% w/v PLGA matrix decreases as CEL2:PLGA ratio increases. This parameter is related to the interaction between CEL2 particles and polymer matrix; this result suggests that there is no bonding between polymer matrix and CEL2, which tends to create some clots within the structure. Moreover, mostly in case of 5% w/v PLGA composites, the parameter τ decreases significantly as the CEL2:PLGA ratio increases, which means that the time for the sample to recover its initial elongation is faster. This trend can be also attributed to the formation of CEL2 clots, which act as fillers inside the polymer matrix (Zhang du et al, 2009). Considering that the produced biomaterials are proposed for potential applications in bone tissue engineering, it is interesting to point out that the elastic modulus (E_1) of most composite films (Tables 3 and 4) is within the range assessed for human cancellous bone (50-500 MPa; Thompson & Hench.

1998). This is an important finding; in fact, the stiffness mismatch between implanted materials and surrounding bone is the principal cause of implant failure. On the basis of the obtained mechanical results this mismatch is theoretically minimised. Of course, this broad reference range for the elastic modulus gives only a preliminary indication on the mechanical suitability of the biomaterials produced (elastic modulus varies greatly depending on the bone site considered); in view of a real clinical application, the selection of the most appropriate biomaterial to be implanted should take into account the specific bone site of implantation characterized by a narrower range of elastic modulus.

3.2 Fabrication of Composite scaffold

Initially, the optimal dispersion composition for the extrusion was selected on the basis of the viscosity of the mixture. Due to the increase of viscosity once CEL2 particles are added to the polymer solution, only 5% and 10% w/v PLGA solution with 20% w/w CEL2:PLGA ratio could be extruded by PAM system. To set-up the optimal working parameters, the line width of a purposely fabricated a serpentine structure, shown in Figure 3A, B, was analysed according to the mathematical model of the PAM system developed by Vozzi et al. (2002).

As can be seen from Figure 4A, D, the line width of the modelled system seems to mimic the experimental data. In particular, both cases show that the line width decreases as motor speed increases; moreover, the line width increases as air pressure increases, in accordance with the model predictions.

On the basis of these results, a velocity of 4500 μm/s and an air pressure of 80 cbar were selected to fabricate the 2D and 3D structures reported in figures 5A to 5D, because they represented the optimal values to obtain a well defined and reproducible line.

The 3D composite PAM scaffold was obtained with a layer-by-layer process. To avoid the collapse of a new layer on the previous one, a 1% hydrofilm solution in deionised water was

deposited at the end of each layer and then dried with a filtered air flow jet. This sacrificial layer at the end of the fabrication process of each 3D structure was easily removed dipping the entire structure in a bath of deionised water until the complete hydrofilm removal. As it is possible to note, the topology of these structures is well defined and they mimic the CAM file well.

3.3 Mechanical properties of 2D and 3D scaffolds

The mechanical analysis of 2D structures shows that from stress-strain curve (Figure 6A) it is possible to extract two elastic moduli, one related to the weft of scaffolds (low strain elastic modulus, in the first part of the stress strain curve) (Figure 6B) and the other one depending on the material used to fabricate them (for higher strains).

Increasing the complexity of the topological structure that composes the elementary cell unit of the 2D scaffold, the elastic modulus increases. This experimental evidence can be explained with the necessity of higher forces for deforming the cell unit, aligning the sides of the cell to the direction of the applied load (Figures 5A-D).

The elastic modulus of hexagonal and octagonal grids are almost 2 and 3 times higher, respectively, compared to the square grids. This can be put in correlation with the number of sides that have to be aligned to the traction direction, i.e. 2 and 3 sides respectively (Mariani et al, 2006). These findings suggest that, as a rule, the increase of complexity of 2D topological structures leads to higher elastic moduli in the composite porous monolayer.

The 3D bone-like scaffold has an elastic modulus that is the mean of the 3 layers – square, hexagonal and octagonal – that compose this type of structure (Figure 6B).

There is a relative paucity of reports on the assessment of the elastic modulus of highly porous bioactive glass/polymer composites; for the purpose of discussion, it is instructive to briefly mention the most significant studies. Blaker et al. (Blaker et al, 2005) reported an elastic modulus within 0.65-1.2 MPa for 45S5 Bioglass®/poly(D,L-lactic acid) composite scaffolds produced by thermally induced phase separation. Baino et al. (Baino et al, 2009) showed that

the deposition of a CEL2 coating on the struts of a polyurethane foam increased the Young modulus of the scaffold from 0.12 to 1.35 MPa. Gentile et al. (2012) reported that the elastic modulus of freeze-dried porous scaffolds, made of chitosan/gelatin blends containing different amounts of CEL2 particles, could be increased up to 2.1 MPa if the glass content was 70 wt.%. In summary, the bone-like scaffolds produced by PAM in the present work exhibit values of elastic modulus higher than those of bioactive glass/polymer porous composites reported in the literature, although they are still far from those of cancellous bone.

3.4 Biological compatibility

The adhesion and spreading of osteoblasts on a scaffold are the first crucial steps in cell-material interaction. The quality of this process will influence the subsequent cell proliferation and/or differentiation. In our study we decided to investigate cell/material interaction using MG-63 human osteoblast-like cells, which have often been used as a model to investigate osteoblast behaviour (Gentile et al, 2012; Shalumon et al, 2011), and human periosteal derived progenitor cells (PDPCs) as a model of bone precursor cells (Ferretti et al, 2014). PDPCs reside in periosteum inner cambium layer (Chang et al, 2012), are able to differentiate *in vitro* into osteochondral cell types (Ferretti et al, 2014) and *in vivo* play a key role in bone repair (Colnot, 2009). Therefore, PDPCs, which are able to carry intracellular tension through their microfilament network and modulate bone and cartilage growth, are a suitable model for the in vitro testing of scaffolds for osteochondral tissue as well as for bone regeneration strategies (Colnot, 2009; Evans et al, 2013).

On the whole, the cells interacted well with the 3D bone-like scaffolds and did not alter cell behaviour at 48 h and 7 days. An MTT test showed that PDPCs displayed significantly ($p<0.05$) higher viability values in comparison with MG63 (figure 7). A significant ($p<0.05$) increase in

cell proliferation from 48 h to 7 days of culture was detected for both cell types. MTT data were strengthened by SEM examination of MG63 and PDPCs seeded on the 3D-bone-like scaffolds (figures 8(a) to (d)).

At 48 h of culture, MG63 were elongated (figure 8(a)), while PDPCs resulted more star-shaped (figure 8(b)) and spread (figure 8(b) inset). After 7 days of culture both cell type tended to colonise the scaffold's structure and appeared more spread (figures 8(c) and 8(d)). After 7 days, the surface of the scaffold cultured with PDPCs was covered by extracellular matrix.

It is well known that osteogenesis is dependent on an ordered sequence of gene activation, starting with the bmp2 pathway, which usually triggers mRNA runx2 transcription, one of the first factors directing the differentiation of precursor stromal stem cells (i.e. PDPCs) towards an osteoblastic lineage (Marcellini et al, 2012). Figure 9 reports RT-qPCR data detected on cells seeded onto scaffolds as fold regulation over PDPCs cultured under osteogenic stimuli after 7 days of culture. PDPCs seeded onto the scaffolds displayed a significant ($p<0.05$) up-regulation in bmp2, whilst no significant changes in the other osteogenic gene were detected. This suggests that the proposed 3D bone-like scaffold do not alter the initial switch of PDPCs' differentiation towards the osteoblastic phenotype.

4. Conclusion

In this work the influence of CEL2 bioactive glass on the mechanical properties of composite PLGA films was analysed, showing the increase of elastic modulus as the amount of the filler material increased. The CEL2-PLGA dispersions were processed with a microfabrication system (PAM), obtaining 2D structures with a well-defined topology that can be assembled to produce a 3D bone-like scaffold. This 3D structure was produced using a slided bone micro-CT as the template. The microfabricated 2D and 3D composite scaffolds were mechanically and biologically tested. In particular, the mechanical analysis showed that their elastic modulus was in the range of native bone tissue and therefore suitable for bone-tissue engineering applications. This assumption was confirmed by biological testing in which both MG63 and PDPCs were shown to be biocompatible with the tested 3D bone-like structures and, moreover, a detected shift towards osteoblastic differentiation. Further studies addressing the role of the proposed scaffold on bone progenitor cells cultured in an appropriate microenvironment are forecast.

On the basis of these results, composite PAM scaffolds could find a large application in the area of Tissue Engineering and Regenerative Medicine, and also for the development of in-vitro bone tissue models.

References

Baino F, Ferraris M, Bretcanu O, Verné E, Vitale-Brovarone C. Optimization of composition, structure and mechanical strength of bioactive 3-D glass-ceramic scaffolds for bone substitution. J Biomater Appl 2013;27:872-890.

Baino F, Verné E, Vitale-Brovarone C. Feasibility, tailoring and properties of polyurethane/bioactive glass composite scaffolds for tissue engineering. J Mater Sci: Mater Med 2009;20:2189-2195.

Baino F, Vitale-Brovarone C. Three-dimensional glass-derived scaffolds for bone tissue engineering: current trends and forecasts for the future. J Biomed Mater Res A 2011;97:514-535.

Behrens P, Bitter T, Kurz B, Russlies M. Matrix-associated autologous chondrocyte transplantation/implantation (MACT/MACI)--5-year follow-up. The Knee. 2006 Jun;13(3):194-202.

Blaker JJ, Maquet V, Jerome R, Boccaccini AR, Nazhat SN. Mechanically anisotropic PDLLA/Bioglass composite foams as scaffolds for bone tissue engineering. Acta Biomater 2005;1:643-52.

Boccaccini AR, Blaker JJ. Bioactive composite materials for tissue engineering scaffolds. Expert Rev Med Devices. 2005 May;2(3):303-17.

Brittberg M, Peterson L, Sjogren-Jansson E, Tallheden T, Lindahl A. Articular cartilage engineering with autologous chondrocyte transplantation. A review of recent developments. J Bone Joint Surg Am. 2003;85-A Suppl 3:109-15.

Chang H, Knothe Tate ML. Concise review: the periosteum: tapping into a reservoir of clinically useful progenitor cells. Stem Cells Transl. Med. 2012:1, 480–91.

Ciardelli G, Gentile P, Chiono V, Mattioli-Belmonte M, Vozzi G, Barbani N, Giusti P. Enzymatically crosslinked porous composite matrices for bone tissue regeneration. J Biomed Mater Res A. 2010 Jan;92(1):137-51 2

Coleman, J.N.; Cadek, M.; Blake, R.; Nicolosi, V.; Ryan, K.P.; Belton, C.; Fonseca, A.; Nagy, J.B.;, Gunk'ko, Y.K.; Blau, W.J. High performance nanotube-reinforced plastics: understanding the mechanism of strength increase. Advance Functional Mater. 2004.14(8),791–8.

Coleman, J.N.; Khan, U.M.; Gun'ko, Y.K. Mechanical reinforcement of polymers using carbon nanotubes. Adv. Mater. 2006,18, 689-706

Colnot, C. Skeletal cell fate decisions within periosteum and bone marrow during bone regeneration. J. Bone Miner. Res. 2009, 24: 274–82.

Dominici M, Le Blank K, Muller I, Slaper-Cortenbach I, Marini F, Krause D, Deans R, Keating A, Prockop Dj, Horwitz E. Minimal Criteria for deifying multipotent mesenchymal

stem cells. The International Society for Cellular Therapy position statement. Cytotherapy 2006; 8(3): 315-317.

Evans, S. F., Chang, H. & Knothe Tate, M. L. Elucidating multiscale periosteal mechanobiology: a key to unlocking the smart properties and regenerative capacity of the periosteum? Tissue Eng. Part B. Rev. 2013,19:147–59.

Ferretti C, Borsari V, Falconi M, Gigante A, Lazzarini R, Fini M, Di Primio R, Mattioli-Belmonte M. Human Periosteum-Derived Stem Cells for Tissue Engineering Applications: The Role of VEGF. Stem Cell Rev. Stem Cell Rev. 8, 882-90, 2012

Ferretti C, Mattioli-Belmonte M. Periosteum derived stem cells for regenerative medicine proposals: Boosting current knowledge. World J Stem Cells. 2014 Jul 26;6(3):266-77. doi: 10.4252/wjsc.v6.i3.266.

Ferretti C, Vozzi G, Falconi M, Orciani M, Gesi M, Di Primio R, Mattioli-Belmonte M. Role of IGF1 and IGF1/VEGF on human mesenchymal stromal cells in bone healing: two sources and two fates. Tissue Eng Part A. 2014 Sep;20(17-18):2473-82.

Gentile P, Mattioli-Belmonte M, Chiono V, Ferretti C, Baino F, Tonda Turo C, Vitale-Brovarone C, Pashkuleva I, Reis RL, Ciardelli G. Bioactive glass/polymer composite scaffolds mimicking bone tissue. J Biomed Mater Res A 2012;100:2654-67.

Gloria A, De Santis R, Ambrosio L Polymer-based composite scaffolds for tissue engineering. J Appl Biomater Biomech. 2010 May-Aug;8(2):57-67

Jelen C, Mattei G, Montemurro F, De Maria C, Mattioli-Belmonte M, Vozzi G, Bone scaffolds with homogeneous and discrete gradient mechanical properties, Materials Science and Engineering: C. Volume 33, Issue 1, 1 January 2013, Pages 28–36

Jones JR. New trends in bioactive scaffolds: the importance of nanostructure. J Eur Ceram Soc 2009;29:1275-1281.

Kawata S, Sun HB, Tanaka T, Takada K. Finer features for functional microdevices. Nature. 2001 Aug 16;412(6848):697-8.

Kruger TE, Miller AH, Wang J. Collagen scaffolds in bone sialoprotein-mediated bone regeneration. ScientificWorldJournal. 2013 Mar 31;2013:812718.

Landers R, Hübner U, Schmelzeisen R, Mülhaupt R. Rapid prototyping of scaffolds derived from thermoreversible hydrogels and tailored for applications in tissue engineering. Biomaterials. 2002 Dec;23(23):4437-47.

Liu, T.; Phang, I.Y.; Shen, L.; Chow, S.Y.; Zhang, WD. Morphology and mechanical properties of multiwalled carbon nanotubes reinforced nylon-6 composites. Macromolecules, 2004, 37, 7214-7222

Livak, K. J. & Schmittgen, T. D. Analysis of relative gene expression data using real-time quantitative PCR and the 2(-Delta Delta C(T)) Method. Methods 2001;25: 402–8 .

Marcellini, S., Henriquez, J. P. & Bertin, A. Control of osteogenesis by the canonical Wnt and BMP pathways in vivo: cooperation and antagonism between the canonical Wnt and BMP pathways as cells differentiate from osteochondroprogenitors to osteoblasts and osteocytes. Bioessays 2012,34: 953–62.

Mariani M, Rosatini F, Vozzi G, Previti A, Ahluwalia A. Characterization of tissue-engineered scaffolds microfabricated with PAM. Tissue Eng. 2006 Mar;12(3):547-57.

Mattioli-Belmonte M, Vozzi G, Kyriakidou K, Pulieri E, Lucarini G, Vinci B, Pugnaloni A, Biagini G, Ahluwalia A. Rapid-prototyped and salt-leached PLGA scaffolds condition cell morpho-functional behavior. J Biomed Mater Res A. 2008 May;85(2):466-76.

Mattioli-Belmonte, M.; Vozzi, G.; Whulanza, Y.; Seggiani, M.; Fantauzzi, V.; Orsini, G.; Ahluwalia, A. Tuning polycaprolactone–carbon nanotube composites for bone tissue engineering scaffolds. Materials Science and Engineering: C, Volume 32, Issue 2, 1 March 2012, Pages 152-159

Miola M, Vitale-Brovarone C, Mattu C, Verné E. Antibiotic loading on bioactive glasses and glass-ceramics: an approach to surface modification. J Biomater Appl 2012;28:308-319.

Mironov V, Boland T, Trusk T, Forgacs G, Markwald RR..Organ printing: computer-aided jet-based 3D tissue engineering. Trends Biotechnol. 2003 Apr;21(4):157-61.

Murphy WL, McDevitt TC, Engler AJ. Materials as stem cell regulators. Nat Mater. 2014 Jun;13(6):547-57.

Pavesio A, Abatangelo G, Borrione A, Brocchetta D, Hollander AP, Kon E, Torasso F, Zanasi S, Marcacci M. Hyaluronan-based scaffolds (Hyalograft C) in the treatment of knee cartilage defects: preliminary clinical findings. Novartis Foundation symposium. 2003;249:203-17; discussion 29-33, 34-8, 39-41.

Pietrzak WS, Perns SV, Keyes J, Woodell-May J, McDonald NM. Demineralized bone matrix graft: a scientific and clinical case study assessment. J Foot Ankle Surg. 2005 Sep-Oct;44(5):345-53.

Rajangam T, An SS. Fibrinogen and fibrin based micro and nano scaffolds incorporated with drugs, proteins, cells and genes for therapeutic biomedical applications. Int J Nanomedicine. 2013;8:3641-62.

Renghini C, Giuliani A, Mazzoni S, Brun F, Larsson E, Baino F, Vitale-Brovarone C. Microstructural characterization and in vitro bioactivity of porous glass-ceramic scaffolds for bone regeneration by synchrotron radiation X-ray microtomography. J Eur Ceram Soc 2013;33:1553-1565.

Rezwan K, Chen QZ, Blaker JJ, Boccaccini AR. Biodegradable and bioactive porous polymer/inorganic composite scaffolds for bone tissue engineering. Biomaterials 2006;27:3413-3431.

Rossi F, Santoro M, Perale G. Polymeric scaffolds as stem cell carriers in bone repair. J Tissue Eng Regen Med. 2013 Nov 6. doi: 10.1002/term.1827

Shalumon KT, Anulekha KH, Chennazhi KP, Tamura H, Nair SV, Jayakumar R. Fabrication of chitosan/poly(caprolactone) nanofibrous scaffold for bone and skin tissue engineering. Int J Biol Macromol. 2011 May 1;48(4):571-6.

Sharma B, Williams CG, Khan M, Manson P, Elisseeff JH. In vivo chondrogenesis of mesenchymal stem cells in a photopolymerized hydrogel. Plast Reconstr Surg. 2007 Jan;119(1):112-20.

Shi X, Sitharaman B, Pham QP, Liang F, Wu K, Edward Billups W, Wilson LJ, Mikos AG, Fabrication of porous ultra-short single-walled carbon nanotube nanocomposite scaffolds for bone tissue engineering, Biomaterials. 2007 Oct;28(28):4078-90.

Siggers K, Frei H, Fernlund G, Rossi F. Effect of bone graft substitute on marrow stromal cell proliferation and differentiation. J Biomed Mater Res A. 2010 Sep 1;94(3):877-85.

The Burden of musculoskeletal conditions at the start of the new millennium. WHO Technical Report Series (http://whqlibdocwhoint/trs/WHO_TRS_919pdf) 2003;919:1-228

Thompson ID, Hench LL. Mechanical properties of bioactive glasses, glass-ceramics and composites. Proc Inst Mech Eng H 1998;212:127-37.

Thomson RC, Giordano GG, Collier JH, Ishaug SL, Mikos AG, Lahiri-Munir D, Garcia CA. Manufacture and characterization of poly(alpha-hydroxy ester) thin films as temporary substrates for retinal pigment epithelium cells. Biomaterials. 1996 Feb;17(3):321-7

Tirella A, De Maria C, Criscenti G, Vozzi G, Ahluwalia A, The PAM2 system: a multilevel approach for fabrication of complex three-dimensional microstructures, Rapid Prototyping Journal 2012;4;229-307

Veetil JV, Ye K. Tailored carbon nanotubes for tissue engineering applications. Biotechnol Prog. 2009 May-Jun;25(3):709-21

Vindigni V, Cortivo R, Iacobellis L, Abatangelo G, Zavan B.Hyaluronan benzyl ester as a scaffold for tissue engineering. Int J Mol Sci. 2009 Jul 3;10(7):2972-85.

Vitale-Brovarone C, Baino F, Verné E. High strength bioactive glass-ceramic scaffolds for bone regeneration. J Mater Sci: Mater Med 2009;20:643-653.

Vozzi G, Ahluwalia A, Rapid Prototyping Methods for Tissue Engineering Applications, in Biomaterials fabrication and processing handbook, edited by P. K. Chu and X. Liu, CRC press 2008 pp.95-114.

Vozzi G, Previti A, Ciaravella G, Ahluwalia A., Microfabricated fractal branching networks, J Biomed Mater Res A. 2004 Nov 1;71(2):326-333

Vozzi G, Previti A, De Rossi D, Ahluwalia A, Microsyringe-Based Deposition of Two-Dimensional and Three-Dimensional Polymer Scaffolds with a Well-Defined Geometry for Application to Tissue Engineering, Tissue Eng. 2002 Dec;8(6):1089-1098.

Whulanza Y, Battini E, Vannozzi L, Vomero M, Ahluwalia A, Vozzi G, Electrical and Mechanical Characterisation of single wall carbon nanotubes based composites for tissue engineering applications, Journal of nanoscience and nanotechnology, J Nanosci Nanotechnol. 2013 Jan;13(1):188-97.

Williams DF. To engineer is to create: the link between engineering and regeneration. Trends Biotechnol. 2006 Jan;24(1):4-8.

Yang W, Both SK, van Osch GJ, Wang Y, Jansen JA, Yang F. Performance of different three-dimensional scaffolds for in vivo endochondral bone generation. Eur Cell Mater. 2014 Jun 10;27:350-64.

Zhang du J, Zhang LF, Xiong ZC, Bai W, Xiong CD. Preparation and characterization of biodegradable poly(D,L-lactide) and surface-modified bioactive glass composites as bone repair materials. J Mater Sci Mater Med. 2009 Oct;20(10):1971-8

Figure

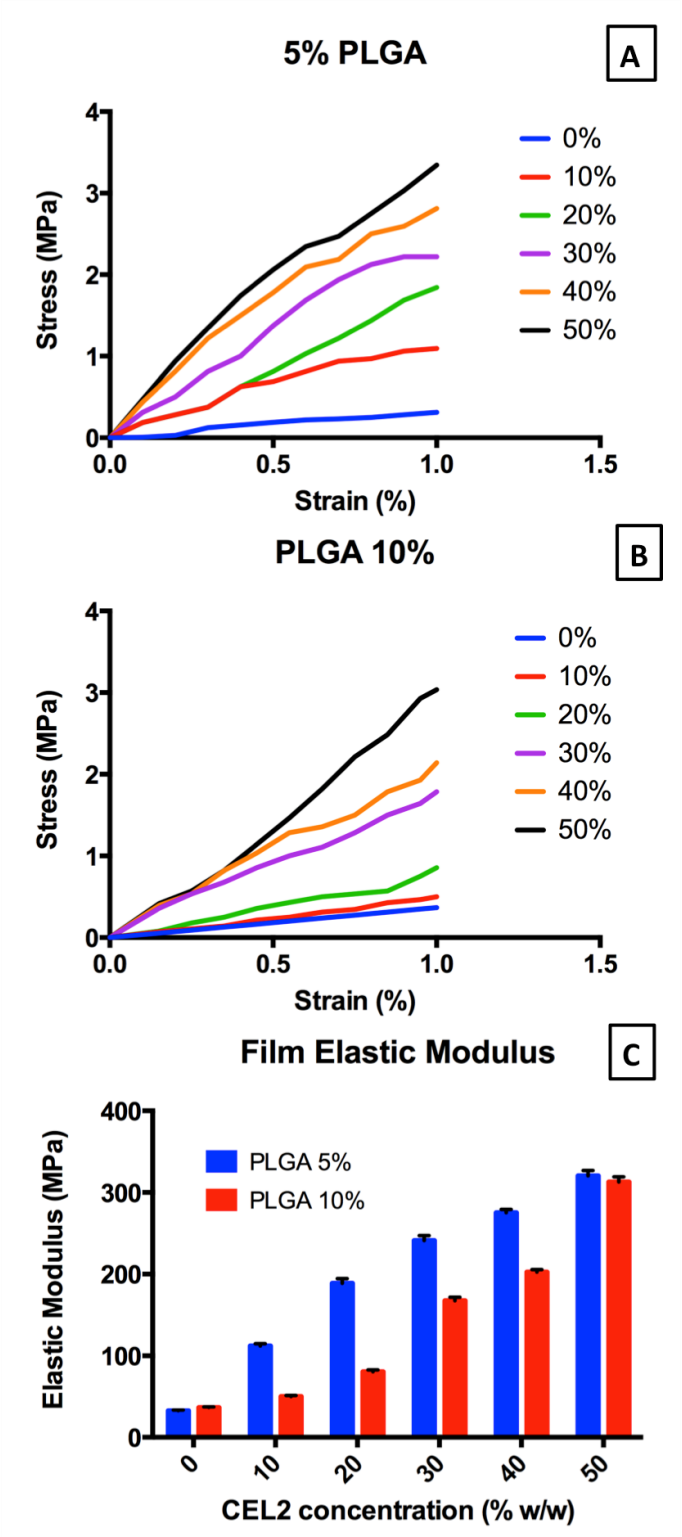

Figure 1: mechanical characterization of PLGA/CEL2 composite: stress-strain curves for 5% PLGA (A) and 10% PLGA (B), and the elastic modulus evaluated as the slope of the first linear part of the stress-strain curves (C)

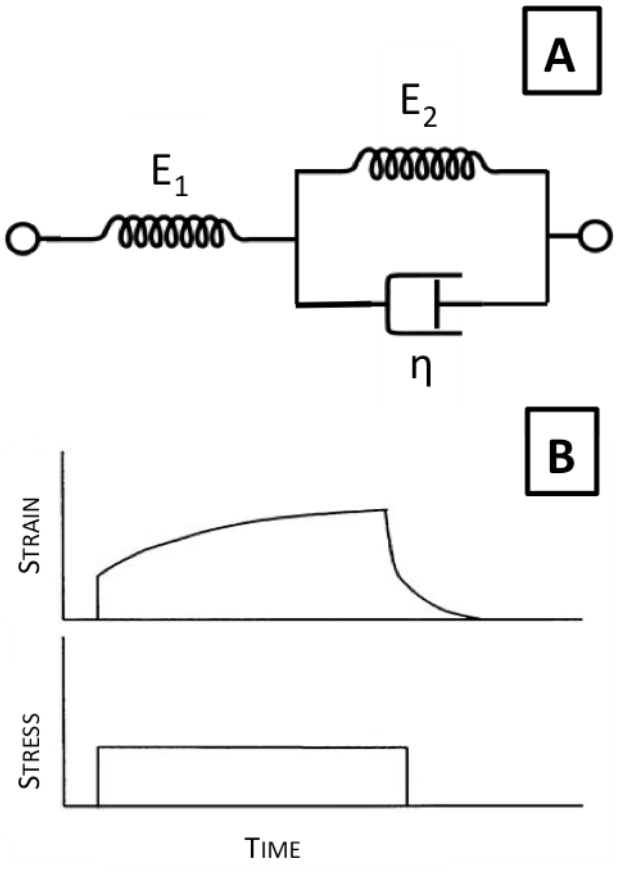

Figure 2: the standard linear elastic solid model (A) and its typical response to a creep test (B)

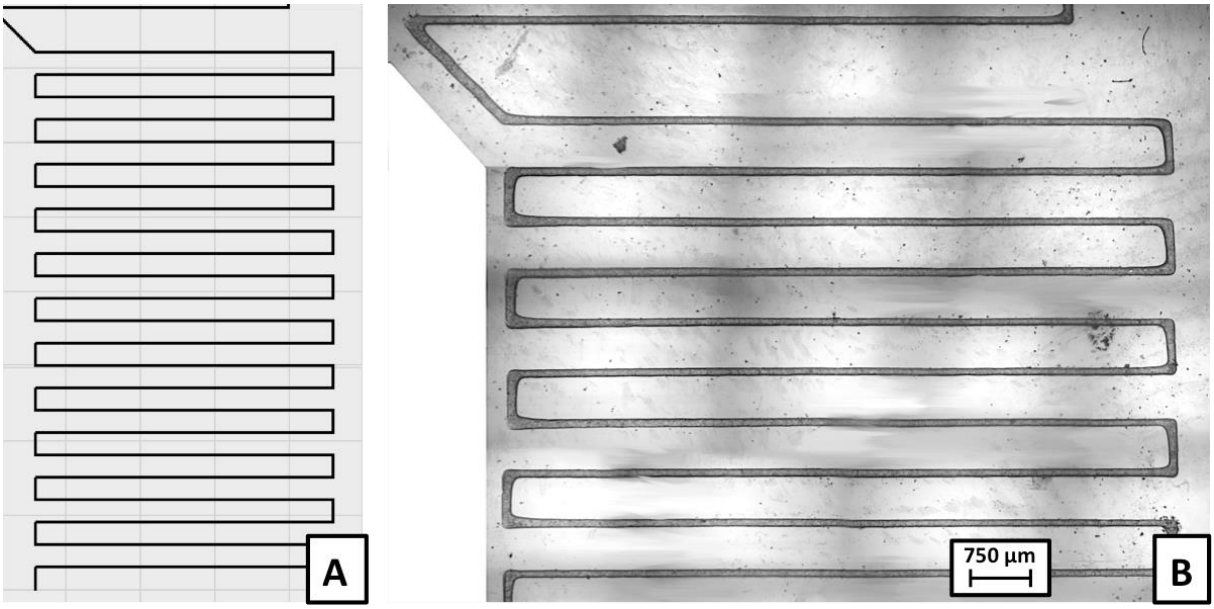

Figure 3: the serpentine tool-path used for calibration: the desired (A) and the experimental geometry (B)

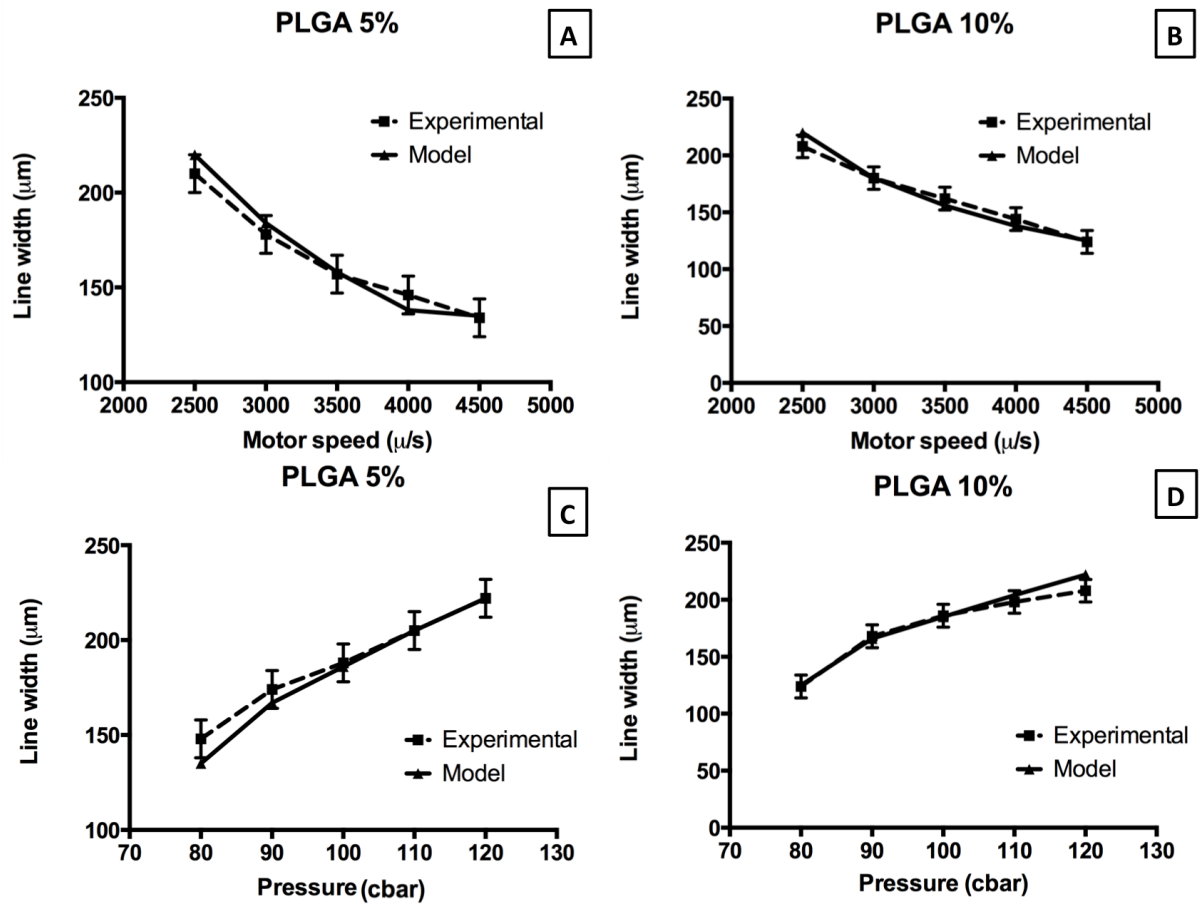

Figure 4: comparison between theoretical and experimental values of line with for different motor speeds (A, B) and different extrusion pressure (C,D)

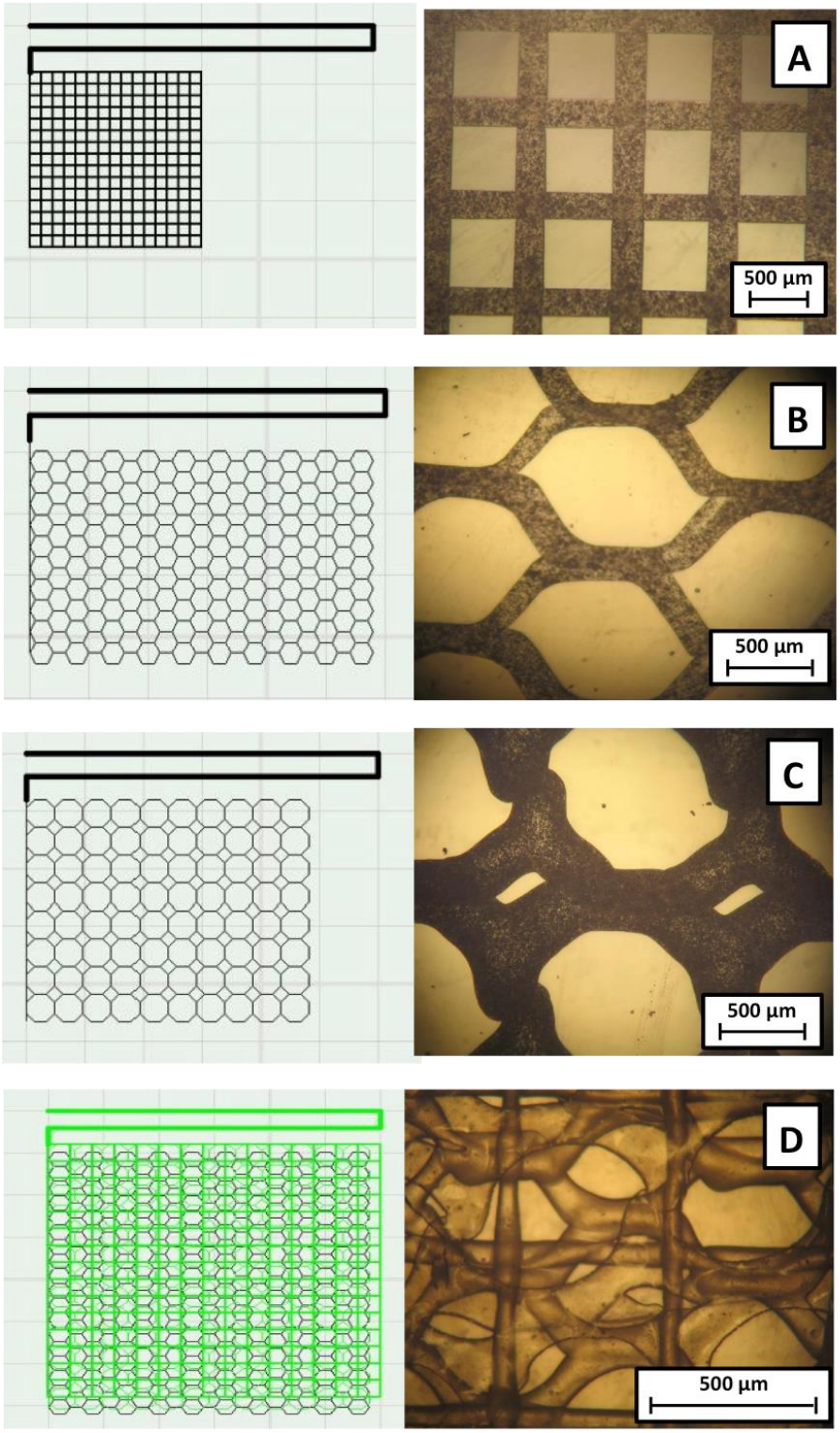

Figure 5: examples of fabricated geometries (for each example the CAD model and the actual structure are presented): square grid (A), hexagonal grid (B) octagonal and rhomboidal grid (C), and bone like scaffold (D)

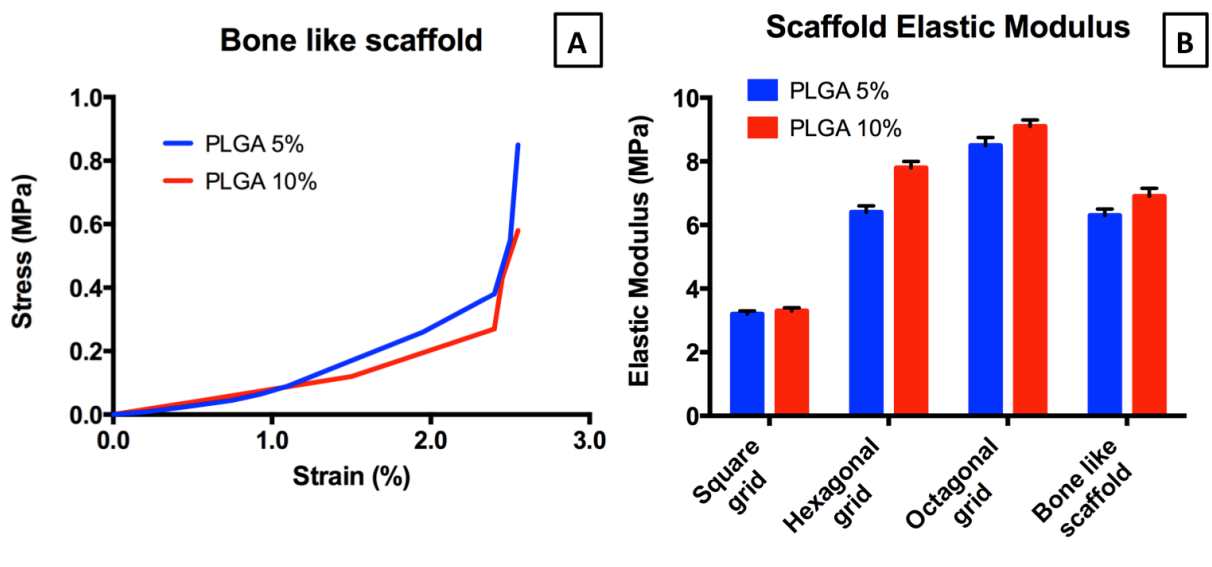

Figure 6: mechanical characterization of 2D and 3D scaffolds, which contains 20% w/w CEL2: the stress-strain curves for 5% PLGA and 10% PLGA for the bone-like scaffold (A) and, the histogram of low strain elastic modulus, related to geometry of the scaffold, valuated as the slope of the first linear part of the stress-strain curves (B).

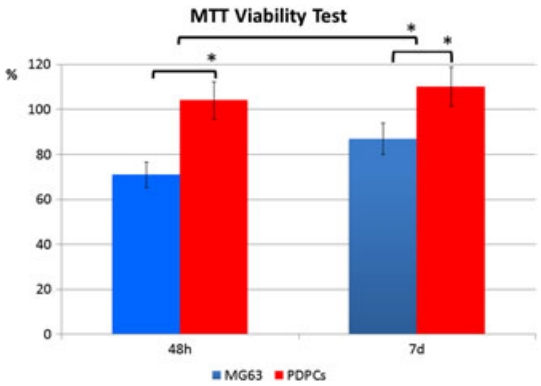

Figure 7: Histogram of MTT test performed on MG63 and PDPCs cultured for 48h and 7 days. *p<0.05

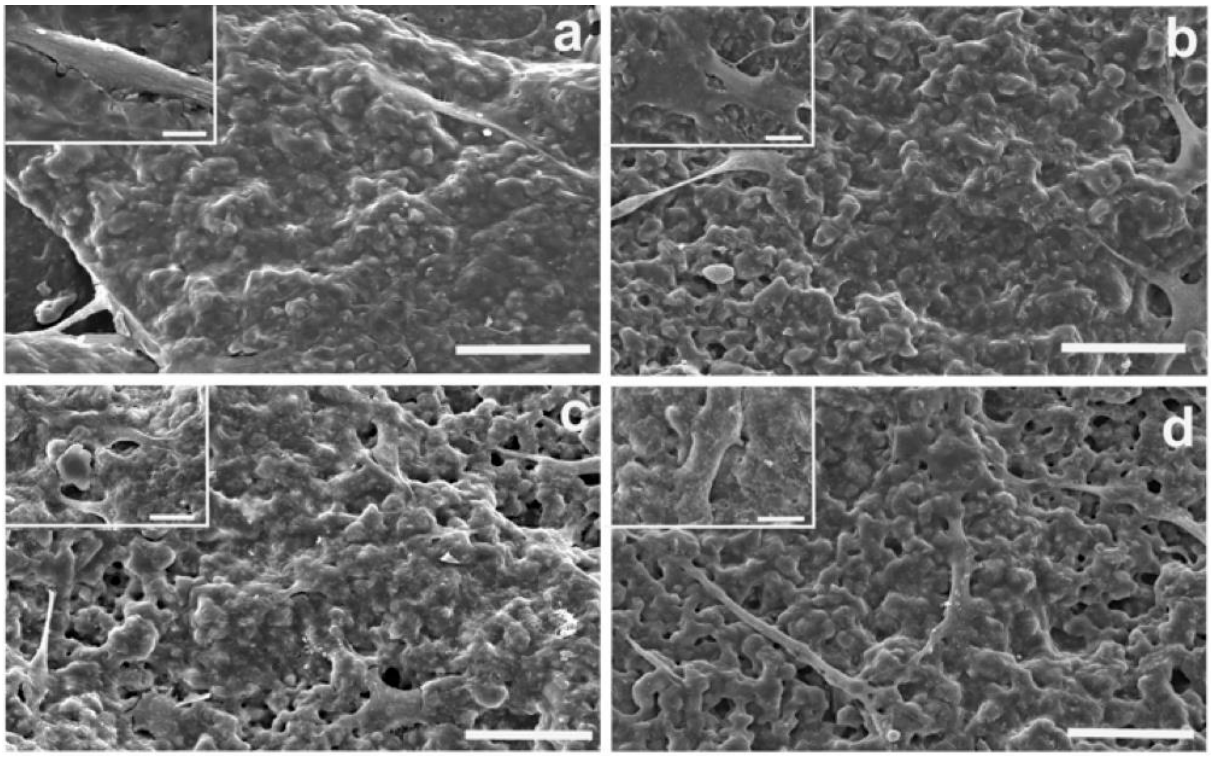

Figure 8: SEM images of MG63 (a,c) and PDPCs (b,d) cultured for 48h (a,b) and 7 days (c,d) onto 3D bone-like scaffolds. Scale bars 50µm; inset scale bars 10µm.

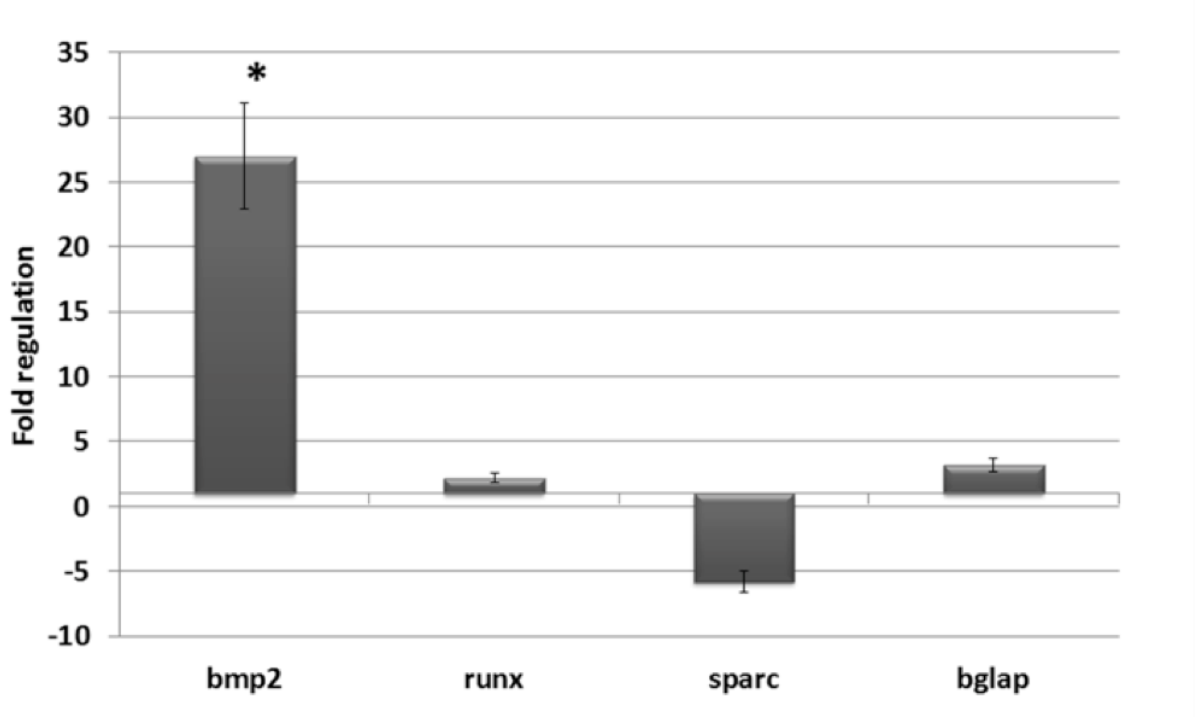

Figure 9

Histograms depict changes in bmp2, runx2, osteonectin (sparc) and osteocalcin (bglap) mRNAs expression in PDPCs cultured for 7 days on the 3D bone-like scaffolds. Data are expressed as Fold-regulation that represents fold-change results in a biologically expressive manner. Fold-regulation is equal to the fold-change (2^(-ΔΔCt)) for fold-change values greater than one and indicate an up-regulation. Fold-change values less than one indicate a down-regulation; in this case the fold-regulation is the negative inverse of the fold-change. *p< 0.05 vs CTRL

Tables

Table 1: Tested composite materials

Composite materials	% (w/v) PLGA solution	% (w/w) CEL2/PLGA ratio
A	5	10
B	5	20
C	5	30
D	5	40
E	5	50
F	10	10
G	10	20
H	10	30
I	10	40
L	10	50

Table 2: Analysed gene description

Genes	**Detected Transcript**	**Primer Forward (5'->3')**	**Primer Reverse (5'->3')**	**Amplicon length (bp)**	**Annealing T (°C)**
RUNX2	**NM_004348.3**	CTCGTCCGCACC GACAGCC	TACCTCTCCGAGG GCTACCACC	111	60°

BMP2	**NM_001200.2**	CCAGCCGAGCCA ACACTGTGC	TCTCCGGGTTGTT TTCCCACTCG	86	60°
SPARC	**NM_003118.3**	TGTTGTCCTCAT CCCTCTCA	CAAGAAGGGCCA CAAGCTC	160	60°
BGLAP	**NM_199173**	GACTGTGACGAG TTGGCTGA	GCCCACAGATTCC TCTTCTG	119	64°
GAPDH*	**NM_002046.3**	AGCCACATCGCT CAGACAC	GCCCAATACGAC CAAATCC	200	60°
*reference gene					

Table 3: Linear standard model parameters for 5% (w/v) PLGA composite material

Composite	E_1 (MPa)	E_2 (MPa)	η (GPa*s)	τ (s)
5% (w/v) PLGA	46.5 ± 1.47	85.1 ± 3.34	34.07 ± 4.66	258.9 ± 44.9
A	183.33 ± 6.43	69.53 ± 2.57	19.87 ± 1.81	78.6 ± 9.6
B	313.33 ± 2.52	73.8 ± 11.78	30.2 ± 0.44	78.0 ± 4.0
C	336.67 ± 22.74	45.77 ± 5.44	23.67 ± 3.06	61.9 ± 12.6
D	330.33 ± 1.53	57.53 ± 7.6	28.5 ± 6.26	73.5 ± 17.9
E	461.17 ± 2.93	73.2 ± 2.43	41.87 ± 3.41	78.4 ± 7.2

Table 4: Linear standard model parameters for 10% (w/v) PLGA composite material

Composite	E_1 (MPa)	E_2 (MPa)	η (GPa*s)	τ (s)
10% (w/v) PLGA	35.59 ± 4.2	63.93 ± 1.18	9.17 ± 0.32	92.1 ± 8.2
F	53.7 ± 3.97	40.97 ± 1.42	9.73 ± 0.12	102.8 ± 7.1
G	83.3 ± 4.6	37.83 ± 0.88	19.2 ± 2.65	158.5 ± 29.1
H	166.67 ± 1.83	36.8 ± 0.6	24.3 ± 1.01	119.4 ± 6.4
I	206.67 ± 4,53	22.56 ± 0.6	29.93 ± 1.45	130.6 ± 9.2
L	312.33 ± 1.37	21.37 ± 0.57	32.67 ± 1.35	97.9 ± 4.6